Histone H2B monoubiquitination regulates heart development via epigenetic control of cilia motility

Andrew Robson[a,b,c,1,2], Svetlana Z. Makova[b,1], Syndi Barish[c], Samir Zaidi[c,3], Sameet Mehta[c], Jeffrey Drozd[b], Sheng Chih Jin[c,4], Bruce D. Gelb[d,e], Christine E. Seidman[f,g,h], Wendy K. Chung[i,j], Richard P. Lifton[c,k], Mustafa K. Khokha[a,b,c,5], and Martina Brueckner[b,c,5]

[a]Pediatric Genomics Discovery Program, Yale University School of Medicine, New Haven, CT 06510; [b]Department of Pediatrics, Yale University School of Medicine, New Haven, CT 06510; [c]Department of Genetics, Yale University School of Medicine, New Haven, CT 06510; [d]The Mindich Child Health and Development Institute, Icahn School of Medicine at Mount Sinai, New York, NY 10029; [e]Department of Pediatrics, Icahn School of Medicine at Mount Sinai, New York, NY 10029; [f]Division of Cardiovascular Medicine, Brigham and Women's Hospital, Boston, MA 02115; [g]Department of Genetics, Harvard Medical School, Boston, MA 02115; [h]Howard Hughes Medical Institute, Chevy Chase, MD 20815; [i]Department of Pediatrics, Columbia University Medical Center, New York, NY 10032; [j]Department of Medicine, Columbia University Medical Center, New York, NY 10032; and [k]Laboratory of Human Genetics and Genomics, Rockefeller University, New York, NY 10065

Edited by Clifford J. Tabin, Harvard Medical School, Boston, MA, and approved May 20, 2019 (received for review May 14, 2018)

Genomic analyses of patients with congenital heart disease (CHD) have identified significant contribution from mutations affecting cilia genes and chromatin remodeling genes; however, the mechanism(s) connecting chromatin remodeling to CHD is unknown. Histone H2B monoubiquitination (H2Bub1) is catalyzed by the RNF20 complex consisting of RNF20, RNF40, and UBE2B. Here, we show significant enrichment of loss-of-function mutations affecting H2Bub1 in CHD patients (enrichment 6.01, $P = 1.67 \times 10^{-03}$), some of whom had abnormal laterality associated with ciliary dysfunction. In *Xenopus*, knockdown of *rnf20* and *rnf40* results in abnormal heart looping, defective development of left–right (LR) asymmetry, and impaired cilia motility. Rnf20, Rnf40, and Ube2b affect LR patterning and cilia synergistically. Examination of global H2Bub1 level in *Xenopus* embryos shows that H2Bub1 is developmentally regulated and requires Rnf20. To examine gene-specific H2Bub1, we performed ChIP-seq of mouse ciliated and nonciliated tissues and showed tissue-specific H2Bub1 marks significantly enriched at cilia genes including the transcription factor *Rfx3*. Rnf20 knockdown results in decreased levels of *rfx3* mRNA in *Xenopus*, and exogenous *rfx3* can rescue the Rnf20 depletion phenotype. These data suggest that Rnf20 functions at the *Rfx3* locus regulating cilia motility and cardiac situs and identify H2Bub1 as an upstream transcriptional regulator controlling tissue-specific expression of cilia genes. Our findings mechanistically link the two functional gene ontologies that have been implicated in human CHD: chromatin remodeling and cilia function.

cilia | ubiquitination | congenital heart disease | RNF20 | histones

Congenital heart disease (CHD), a structural abnormality of the heart and/or great vessels, affects ∼1% of live born infants. Despite survival of 90% of CHD patients to adulthood, CHD remains the leading cause of birth defect-related mortality in the United States and Europe (1). Whole-exome sequencing (WES) of CHD patients identified de novo mutations (DNMs) affecting chromatin modifications (including H3K4 and H3K27 methylation and H2BK120 ubiquitination) contributing to 2–3% of CHD (2–5). While the mechanism(s) by which H3K4 and H3K27 methylation impact heart development is being investigated (6, 7), the role of monoubiquitination of histone H2B on K120 (H2Bub1) in heart development is unknown. H2Bub1 is linked to down-regulation of pluripotency factors in ES cell differentiation (8–10). In mammals, H2Bub1 is catalyzed by the RNF20–RNF40 complex together with the ubiquitin-conjugating enzyme UBE2B (11) (*SI Appendix*, Fig. S1*A*).

In addition to mutations affecting chromatin-remodeling genes, genomic analysis of CHD patients (3) and a genetic screen in mice (12) reveal a significant contribution from recessive mutations affecting cilia. Cilia are hair-like organelles found on the surface of most vertebrate cells and serve functions including signaling and extracellular fluid propulsion. In heart development, the best understood role for cilia is establishing left–right (LR) asymmetry and determining the direction of heart looping. A highly conserved ciliated left–right organizer (LRO) utilizes motile and immotile cilia to generate and sense directional flow of extraembryonic fluid and transduce it to a calcium signal (13–16). Defects affecting cilia motility result in heterotaxy (Htx) (associated with CHD); 6.5% of patients with PCD (primary ciliary dyskinesia), a disorder defined by abnormal cilia motility in the airway epithelia (17), also display Htx and CHD (18).

Significance

Congenital heart disease affects 1% of infants, and variants were identified affecting genes (*RNF20*, *RNF40*, and *UBE2B*) involved in a chromatin modification called histone 2B monoubiquitination (H2Bub1). How these variants lead to congenital heart disease remains unknown. Here, we demonstrate how H2Bub1 pathway modulation during development leads to abnormal cardiac left–right patterning. In *Xenopus*, H2Bub1 regulates cilia motility, and defects lead to abnormal inner dynein arms, mirroring a patient with an *RNF20* mutation. Moreover, we show that H2Bub1 marks are enriched on the cilia transcription factor *Rfx3* in a tissue-specific manner; furthermore, addition of *rfx3* mRNA to Rnf20-depleted embryos restores cilia motility. Thus, our findings uncover a mechanism linking H2Bub1 with cilia and cardiac development.

Author contributions: A.R., S.Z.M., M.K.K., and M.B. designed research; A.R., S.Z.M., S.B., S.Z., J.D., S.C.J., M.K.K., and M.B. performed research; S.C.J., B.D.G., C.E.S., W.K.C., and M.B. contributed new reagents/analytic tools; A.R., S.Z.M., S.B., S.Z., S.M., S.C.J., R.P.L., M.K.K., and M.B. analyzed data; and A.R., S.Z.M., S.B., M.K.K., and M.B. wrote the paper.

The authors declare no conflict of interest.

This article is a PNAS Direct Submission.

Data deposition: Final RNA-seq and processed data resulting from the ChIP-seq experiments reported in this paper have been deposited in the Gene Expression Omnibus (GEO) database, https://www.ncbi.nlm.nih.gov/geo (accession nos. GSE132115–GSE132117, and GSM3844810–GSM3844844).

[1]A.R. and S.Z.M. contributed equally to this work.

[2]Present address: Sir William Dunn School of Pathology, Oxford OX3 9DU, United Kingdom.

[3]Present address: Department of Medicine, Memorial Sloan Kettering Cancer Center, New York, NY 10065.

[4]Present address: Laboratory of Human Genetics and Genomics, Rockefeller University, New York, NY 10065.

[5]To whom correspondence may be addressed. Email: mustafa.khokha@yale.edu or martina.brueckner@yale.edu.

This article contains supporting information online at www.pnas.org/lookup/suppl/doi:10.1073/pnas.1808341116/-/DCSupplemental.

Published online June 24, 2019.

The structure of the cilium is tightly regulated in part by transcription factors (TFs), such as FoxJ1, Rfx2, and Rfx3 (19–23). Rfx3 binds to promoters of many cilia genes, including *Foxj1*, *Dnah9*, and *Dnah5* (20). Rfx2 functions in LR asymmetry development in zebrafish (22) and *Xenopus* (23). Finally, FoxJ1 and Rfx2 bind cooperatively at chromatin loops and promote gene expression in multiciliated cells (MCCs) (24). While our knowledge of the TFs that regulate ciliogenesis is emerging, the chromatin modifications that regulate these factors are mostly unexplored.

Here, we demonstrate that the RNF20–RNF40 E3 ligase complex together with UBE2B (the RNF20 core complex) regulates H2Bub1 during development and affects transcription of cilia genes required for LR patterning and cardiac development. Rnf20 depletion in *Xenopus* leads to reduced expression of *rfx3* at the left–right organizer, cilia dysmotility, and abnormal LR development. H2Bub1 marks are enriched at cilia genes in mouse multiciliated tissues, including at the *Rfx3* locus. Together, our results identify the RNF20 complex as a transcriptional regulator of cilia genes and identify one mechanism by which it regulates cardiac development.

Results

Dominant Mutations Affecting H2Bub1 Are Associated with CHD and Abnormal Laterality. CHD has extensive underlying heterogeneity; by WES, we identified three CHD patients with monoallelic mutations (RNF20 and UBE2B de novo and RNF40 inherited) affecting the RNF20 core complex (Fig. 1*A* and *SI Appendix*, Fig. S1) (3). All three variants (hg19 reference genome) are absent from the gnomAD database, suggesting that these mutations are under strong selection pressure and likely disease-causing. The *RNF20* and *RNF40* variants are predicted to result in loss of function (LoF), while the missense R8T *UBE2B* variant changes a charged to an uncharged residue at a predicted interaction site

A

Patient	Gene	Inheritance	Protein	CHD
1	RNF20	*de-novo*	p.Q83X	Dextrocardia, RAI, TAPVR, CAVC, PA, L-TGA
2	RNF40	inherited	Splice, exon 4-5 (c.138+1G>A)	HLHS
3	UBE2B	*de-novo*	p.R8T	TOF, RAA

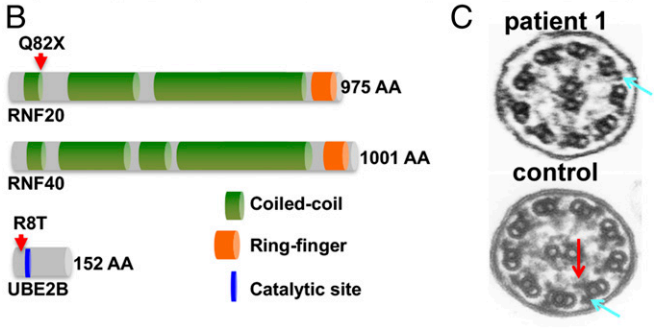

Fig. 1. Mutations affecting the core RNF20 complex are identified in patients with congenital heart disease. (*A*) Summary of patient variants, inheritance, and phenotypes affecting the core components of the RNF20 complex (RNF20, RNF40, and UBE2B). CAVC, complete atrioventricular canal; HLHS, hypoplastic left heart syndrome; L-TGA, levo-transposition of the great arteries; PA, pulmonary atresia; RAA, right aortic arch; RAI, right atrial isomerism; TAPVR, total anomalous pulmonary venous return; TOF, tetralogy of Fallot. (*B*) Diagrams of RNF20, RNF40, and UBE2B with patient variants (red arrows) indicated. (*C*) TEM of tracheal cilia from a patient with the *RNF20* variant (*Top*) and control (*Bottom*). Blue arrows point to outer dynein arms; the red arrow points to IDAs. High-magnification electron micrographs were obtained from greater than 10 ciliated cells.

of RNF20 and UBE2B (Fig. 1*B*) (25). The core complex interacts directly or indirectly with other proteins including the PAF1 complex to regulate H2Bub1, and/or link H2Bub1 to other chromatin modifications. To evaluate the contribution to CHD of genes outside the RNF20 core complex affecting H2Bub1, we identified 45 RNF20 core complex-interacting genes from STRING (*SI Appendix*, Fig. S2*A*). We then used de novo expectation analysis of the previous WES analysis of 2,645 CHD proband–parent trios and 1,789 control–parent trios (unaffected siblings of autism patients) (phs000571.v1.p1, phs000571.v2.p1, and phs000571.v3.p2) (3, 26, 27) to test for enrichment in DNMs comparing observed to expected DNMs. We identified significant enrichment in LoF and protein-altering and -damaging (LoF + damaging missense, defined as MetaSVM-damaging) DNMs affecting the RNF20-interactome genes in CHD patients but not in controls (Table 1).

The phenotypes of the patients with DNMs affecting H2Bub1 encompassed the full range of CHD (*SI Appendix*, Fig. S2 and Table S1). Five of 14 patients with DNMs affecting H2Bub1, including two patients with variants affecting the core RNF20 complex, had LR defects. The patient with the *RNF20* variant, and no biallelic mutation in known PCD genes, presented with cardiac disease characteristic of Htx (Fig. 1*A*). In addition to CHD, the *RNF20* patient had chronic respiratory failure and recurrent pulmonary infections with organisms including *Pseudomonas*, *Stenotrophomonas*, and *Serratia*, hydrocephalus with enlargement of the lateral and third ventricles, and biopsy of tracheal cilia demonstrating absent inner dynein arms (IDAs) (Fig. 1*C*), similar to a previous report (28).

***rnf20* Depletion Alters LR Development in *Xenopus*.** LR patterning is conserved across vertebrates, so we utilized *Xenopus* to evaluate the role of Rnf20 in LR development. Since global knockdown of *rnf20* by injecting morpholino oligo (MO) at the one-cell stage leads to edema by stage 40 (*SI Appendix*, Fig. S4*A*), precluding analysis of heart looping, we injected the *rnf20* MO in one cell of the two-cell embryo and scored cardiac looping. In *Xenopus*, injection of one blastomere at the two-cell stage allows targeting *rnf20* knockdown to either the left or right side of an embryo (*SI Appendix*, Fig. S3). Normal heart looping (D loop; *SI Appendix*, Fig. S4*B*, *i*) positions the outflow to the right of the inflow; reversed heart looping positions the outflow to the left of the inflow (L loop; *SI Appendix*, Fig. S4*B*, *ii*); and absent heart looping (A loop) positions the outflow and inflow at the midline. Previous work showed that cilia function on the left side of the *Xenopus* LRO is essential for LR patterning, while cilia function on the right appears dispensable (29). *rnf20* depletion led to significantly more cardiac looping abnormalities (16% in the left and 9% in the right), compared with uninjected controls (Ctrl; 0%) (Fig. 2*A*). More abnormal heart loops resulting from left-sided injection suggested that one function of Rnf20 in LR development is through LRO cilia function. To determine at which step in LR development Rnf20 is required, we examined global markers of LR asymmetry, *pitx2c* and *dand5* (also called *coco* in *Xenopus* and *cerl2* in mouse). *pitx2c* is normally expressed in the left lateral plate mesoderm (30). *rnf20* depletion at the one-cell stage led to abnormal *pitx2c* expression at stage 28 (44% of embryos, compared with 2.5% of Ctrl embryos) (Fig. 2*B*). Left-sided *rnf20* depletion led to more *pitx2c* expression abnormalities (53%, left depletion, compared with 26%, right depletion), which is consistent with the heart-looping observation (Fig. 2*A*). *dand5* is a nodal antagonist whose transcripts are degraded on the left side of the LRO in response to normal LRO ciliary function (31). *rnf20* knockdown at the one-cell stage resulted in significantly more abnormal (bilateral, left, or absent; outlined in *SI Appendix*, Fig. S3) *dand5* mRNA expression at stage 19 (33%) compared with Ctrl (9%) (Fig. 2*B*), which is consistent with the abnormal *pitx2c* expression pattern resulting from either one-cell or left-sided two-cell *rnf20* knockdown.

Table 1. De novo enrichment analysis in 45 RNF20-interactome genes

	Cases, n = 2,645						Controls, n = 1,789					
	Observed		Expected				Observed		Expected			
	N	Rate	N	Rate	Enrichment	P	N	Rate	N	Rate	Enrichment	P
Total	15	0.0057	8.9	0.0034	**1.69**	**0.0381**	6	0.0034	6	0.0034	1	0.55
Syn	1	0.0004	2.4	0.0009	0.41	0.913	1	0.0006	1.6	0.0009	0.61	0.81
Missense	9	0.0034	5.6	0.0021	1.6	0.116	4	0.0022	3.8	0.0021	1.06	0.52
Damaging missense	3	0.0011	1.8	0.0007	1.64	0.278	1	0.0006	1.2	0.0007	0.811	0.71
LoF	5	0.0019	0.8	0.0003	**6.01**	**0.00167**	1	0.0006	0.6	0.0003	1.78	0.43
Protein-altering	14	0.0053	6.5	0.0025	**2.17**	**0.00669**	5	0.0028	4.3	0.0024	1.15	0.44
Protein-damaging	8	0.0030	2.7	0.0010	**3**	**0.00613**	2	0.0011	1.8	0.0010	1.11	0.54

Analyzed were 2,645 CHD case trios and 1,789 control trios (unaffected siblings from autism trios). Significant enrichment is highlighted in bold. Syn is synonymous mutation. Damaging missense mutation is meta-SVM damaging. Protein-damaging is LoF + Damaging missense mutations.

To test the specificity of the *rnf20* MO, we depleted Rnf20 using CRISPR in *Xenopus* and analyzed F0 embryos (32). Targeting the first *rnf20* exon resulted in abnormal *pitx2c* expression in 22% of injected embryos (*SI Appendix*, Fig. S4*C*). Additionally, we partially rescued the *rnf20* MO phenotype with human *Rnf20* mRNA, demonstrating specificity of the *rnf20* MO (*SI Appendix*, Fig. S4*D*). Together, these results indicate that one function of Rnf20 in the development of LR asymmetry lies upstream of *dand5* at the LRO.

***rnf20* Is Expressed in the LRO and Multiciliated Tissues in *Xenopus* and Mouse.** Our findings suggest that RNF20 may affect cilia and potentially link H2Bub1 to cilia. We investigated Rnf20 expression levels in *Xenopus* and mice. *rnf20*, *rnf40*, and *ube2b* mRNAs are broadly expressed early in *Xenopus* development, and then become restricted to midline structures, including the ciliated LRO (*SI Appendix*, Fig. S5*A*). Rnf20 protein is expressed broadly in nuclei of *Xenopus* and mouse embryos, including the LRO and epidermis (*SI Appendix*, Figs. S5 *B* and *C* and S6*A*). Also, Rnf20 protein is found in nuclei of the *Xenopus* epidermis (*SI Appendix*, Fig. S5*C*, *Top*) but not within or near the cilium (*SI Appendix*, Fig. S5*C*, *Bottom*). Since the patient with the *RNF20* mutation also had evidence of PCD, which affects the MCCs, we evaluated RNF20 protein expression in multiciliated tissues (trachea, brain ventricles, and oviduct). Western blot and IF showed prominent RNF20 protein in adult mouse multiciliated tissues, especially in the oviduct, trachea, and brain, with the most prominent localization in MCCs (*SI Appendix*, Fig. S6 *B* and *C*). These data support a role for nuclear Rnf20 in ciliated cells.

Rnf20 Knockdown Affects Ciliary Motility in *Xenopus*. Motile cilia are essential for repressing *dand5* expression on the left of the LRO (31); therefore, we examined *Xenopus* LRO cilia. Depletion of *rnf20* did not change cilia length, number, or orientation at the LRO (*SI Appendix*, Fig. S7*A*). LRO cilia motility was examined by live imaging cilia labeled with Arl13b-mCherry (16). We found no significant change in total number of cilia and ratio of motile/immotile cilia in *rnf20* morphants compared with Ctrl embryos (*SI Appendix*, Fig. S7*A*). However, *rnf20* morphants displayed a significant decrease in rotation frequency suggestive of a motility defect (Fig. 3 *A* and *B* and Movie S1). These results suggested that alterations in cilia motility underlie the LR patterning defects observed in *rnf20* morphants. We then examined the MCCs of the *Xenopus* embryonic epidermis that normally beat coordinately to directionally move extraembryonic fluid. Acetylated tubulin immunostaining (Fig. 3*C*, *Top* and *SI Appendix*, Fig. S7*B*) of *Xenopus* embryos showed normal distribution and morphology of cilia on the surface of *rnf20* morphant MCCs, but cilia motility was impaired, appearing "stiff," with a limited range of motion in *rnf20* morphants (Movie S2); similar stiff cilia motility has previously been reported in the setting of defective IDAs in a PCD patient (33). We analyzed motility of unlabeled and membrane-GFP–labeled epidermal cilia and found labeling had no effect (Movies S2 and S3). We quantified epidermal fluid flow by applying fluorescent beads to the medium and measuring the distance traveled by a bead propelled by cilia. The velocity of beads in proximity to MCCs was significantly reduced in *rnf20* morphants compared with control MO embryos (Fig. 3*D*). F0 CRISPR-based *rnf20* depletion led to a similar change in cilia motility and reduced epidermal fluid flow (Movie S4). TEM of *Xenopus* epidermal cilia ultrastructure of *rnf20*-depleted embryos demonstrated shortened/absent IDAs in 8/8 axonemes examined (Fig. 3*C*, *Bottom*), similar to the patient carrying the *RNF20* variant (Fig. 1*C*); we also observed absent or shortened outer dynein arms (ODAs) in 2/8 axonemes examined. We conclude that *rnf20* is essential for effective cilia motility by regulating ciliary IDAs.

Members of the RNF20 Core Complex Synergistically Affect Cilia Motility and LR Asymmetry Development. RNF20 is a component of the RNF20–40–UBE2B complex, so we investigated whether there is a combinatorial effect on cilia function and LR development resulting from depletion of combinations of RNF20 core complex components. We identified MO doses that did not generate an epidermal cilia phenotype (*rnf20* 1/2, *rnf40* 1/2, and *ube2b*) (Fig. 3*E*), and also resulted in reduced-penetrance LR phenotype based on *pitx2c* mRNA expression (Figs. 2*B* and 3*F*). However, coinjection of *rnf20* 1/2 and *rnf40* 1/2 MOs and

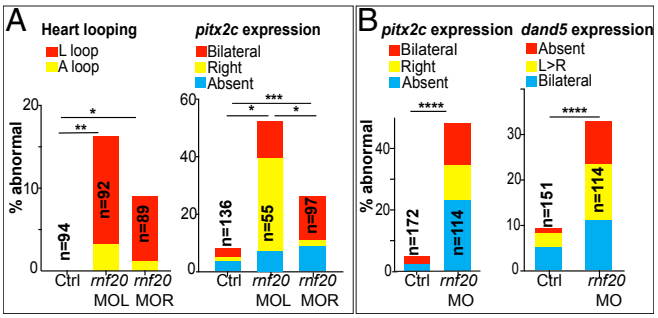

Fig. 2. *Rnf20* depletion in *Xenopus* causes left–right abnormalities. (*A*, *Left*) Percentage of *Xenopus* embryos with abnormal cardiac looping after injection of *rnf20* MO into either the right or left blastomere at the two-cell stage. (*A*, *Right*) Percentage of embryos with abnormal *pitx2c* in one-cell injections of two-cell embryos. MOL, left blastomere injection; MOR, right blastomere injection. *n*, number of embryos from three independent experiments. χ^2/Fisher's exact test, ***$P < 0.0005$, **$P < 0.005$, *$P < 0.05$. (*B*) Expression of LR markers in one-cell–injected embryos. (*B*, *Left*) *pitx2c* expression. (*B*, *Right*) *dand5* expression. *n*, number of embryos from three independent experiments. χ^2/Fisher's exact test, ****$P < 0.00005$.

DEVELOPMENTAL BIOLOGY

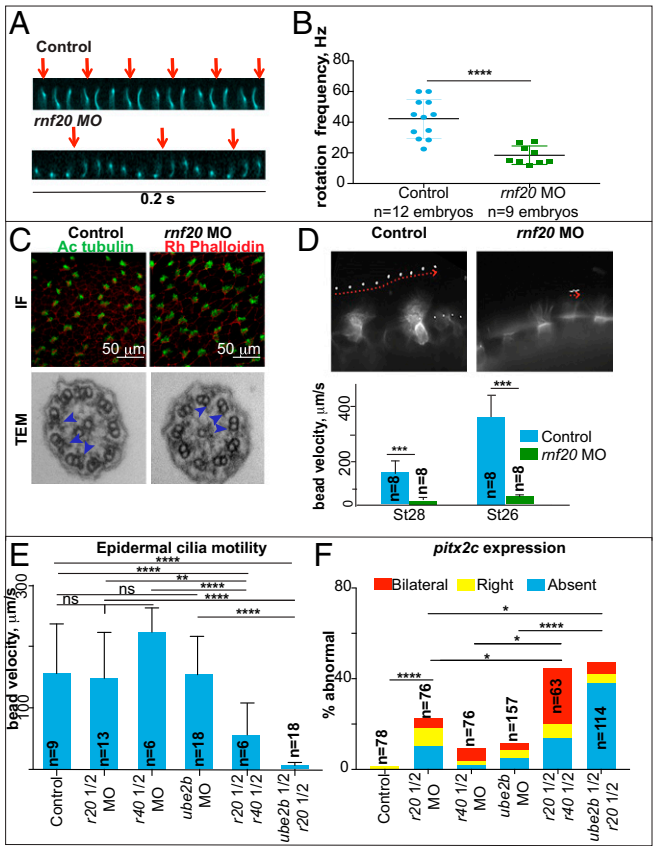

Fig. 3. Cilia motility is impaired in *Xenopus* embryos depleted of components of the RNF20 complex. (*A*) Cilia beat frequency (CBF) in Ctrl and *rnf20* MO LRO explants. Cilia were visualized by expressing Arl13b-GFP. Time-lapse montage of a single cilium. The space between the red arrows represents the number of frames of a ciliary single cycle. (*B*) Quantification of CBF in the LRO in Ctrl and *rnf20* MO-injected embryos. Unpaired *t* test, $^{****}P < 0.00005$. (*C*, *Top*) Lateral view of an embryo with the epidermal multicilia labeled with antiacetylated tubulin and F-actin stained with phalloidin. (*C*, *Bottom*) TEM of *Xenopus* Ctrl and *rnf20* morphant embryo epidermal cilia. IDAs are indicated by blue arrowheads. (*D*, *Top*) Analysis of epidermal cilia motility by tracking the fluorescent bead trajectory on the epidermal surface. Maximum projection of time-lapse images obtained during 0.3 s demonstrates the distance traveled by a bead propelled by motile cilia on the surface of the embryo. (*D*, *Bottom*) Quantification of bead velocity in Ctrl and *rnf20* MO embryos at stages 22 and 26. *n*, number of embryos examined; 10–15 different beads per embryo were followed. Unpaired *t* test, $^{***}P < 0.0005$. (*E*) Quantified bead velocity after suboptimal dose MO (1/2), *rnf20* (*r20*), *rnf40* (*r40*), full-dose *ube2b*, or coinjected suboptimal doses of MO. *n*, number of embryos from three independent experiments. χ^2/Fisher's exact test, $^{****}P < 0.00005$, $^{**}P < 0.005$. ns, not significant. (*F*) Percentage of embryos with abnormal *pitx2c* expression after suboptimal dose MO (1/2), *rnf20*, *rnf40*, full-dose *ube2b*, or coinjected suboptimal doses of MO. *n*, number of embryos from three independent experiments. χ^2/Fisher's exact test, $^{****}P < 0.00005$, $^{*}P < 0.05$. Error bars in *D* and *E* are SD.

coinjection of *ube2b* and *rnf20* 1/2 MOs led to reduced bead velocity over MCCs and abnormal asymmetric *pitx2c* mRNA expression compared with Ctrl and single-gene MO-injected embryos (Fig. 3 *E* and *F* and Movies S5, S6, and S7). MO specificity was tested for the *rnf40* MO both by mRNA rescue and reduction of H2Bub1/H2B ratio (*SI Appendix*, Fig. S4*D*). The *ube2b* MO alone did not result in a change in H2Bub1/H2B or an observable phenotype. This implies that RNF20 core complex members combinatorially affect cilia function and LR patterning.

H2Bub1 Is Dynamic During Development at the Time of LRO Formation. Our findings that the RNF20 complex is required for cilia motility suggest that its effect is via epigenetic control of cilia genes at times crucial to LR asymmetry development and epidermal cilia formation. To determine if H2Bub1 levels are developmentally regulated, we analyzed H2Bub1 and H2B levels in *Xenopus* embryos from stage 12 to 22. The H2Bub1/H2B ratio sharply increased at stage 14 (formation of LRO), remained elevated during LRO stages (16–18), decreased at stage 20, and increased again at stage 22, when formation of epidermal cilia begins (*SI Appendix*, Fig. S8 *A* and *B*). We tested whether Rnf20 is required for H2Bub1 developmental regulation by comparing H2Bub1/H2B in *rnf20* morphant and uninjected Ctrl embryos. The global level of H2Bub1/H2B was lower in *rnf20* morphant embryos at all developmental stages examined (*SI Appendix*, Fig. S8 *A* and *B*), and the peaks in H2Bub1/H2B observed in Ctrl embryos at LRO and epidermal cilia formation stages were completely absent in *rnf20* morphant embryos (*SI Appendix*, Fig. S8 *B* and *C*). These data demonstrate that H2Bub1 is developmentally regulated, and up-regulation correlates with LRO and epidermal cilia formation and requires Rnf20.

H2Bub1 Marks Are Enriched at Cilia Genes in Multiciliated Tissue. Since global H2Bub1 marks do not reflect the specific role of RNF20 complex-mediated H2Bub1 in LR development and CHD, we examined gene-level tissue-specific H2Bub1 marks by chromatin immunoprecipitation followed by high-throughput sequencing (ChIP-seq) of H2Bub1 marks in multiciliated tissue (oviduct) and nonmulticiliated tissue (liver) in mice. Oviduct was selected as a proxy multiciliated tissue because it was amenable to ChIP-seq and has MCCs expressing RNF20 (*SI Appendix*, Fig. S6 *B* and *C*). Oviduct and liver peaks were grouped into clusters based on H2Bub1 occupancy (high, moderate, low, and none) (*SI Appendix*, Fig. S9). Gene ontology (GO) enrichment analysis was performed on the genes in each cluster. The "no" occupancy cluster contained genes not specific to oviduct. The "high" and "moderate" occupancy clusters contained transcription and ubiquitination genes. The "low" occupancy cluster contained cilia genes, many with differing levels of H2Bub1 occupancy in oviduct and liver (*SI Appendix*, Fig. S10*A*).

We next performed a differential binding analysis with the H2Bub1 ChIP-seq data to determine genomic regions with differing H2Bub1 occupancy comparing oviduct and liver. We found 1,067 regions in liver and 836 regions in oviduct with increased occupancy (Dataset S1). GO enrichment analysis on the genes near the regions with increased occupancy in liver indicated that these regions were adjacent to liver-specific genes. Unlike the regions with enriched occupancy in liver, the genes near the enriched regions in oviducts did not contain oviduct-specific GO terms (such as oviduct development or ovulation). Instead, it contained 89 cilia genes, such as *Kif3a* (heterotrimeric kinesin A) and *Rfx3* (Fig. 4*A* and Dataset S1), and 8 GO terms related to cilia and 1 related to LR patterning in the top 20 terms (Fig. 4*B* and *SI Appendix*, Fig. S10*A*). Increased occupancy of *Rfx3* in oviducts was confirmed by ChIP-qPCR (*SI Appendix*, Fig. S10*B*). It is of note that not all cilia gene regions have H2Bub1 marks, including *Dnah7a*, an IDA (Fig. 4*C*). These data identify higher levels of H2Bub1 marks at a subset of cilia genes in multiciliated tissue, and point to H2Bub1 as a transcriptional regulator of ciliary genes.

Rnf20 Regulates Rfx3. We next determined the transcriptional effect of Rnf20 knockdown. We tested expression levels of *rfx3* (a ciliary TF identified in the ChIP-seq dataset), *foxj1* (a ciliary TF not identified in the ChIP-seq dataset), *dnah7* (IDA relevant to the patient phenotype), and *dnah9* and *dnah11* (ODAs) mRNAs at the *Xenopus* LRO. qPCR of dissected *Xenopus* LROs from *rnf20* morphant and control embryos revealed decreased *dnah7* and *rfx3* mRNAs but not *dnah9*, *dnah11*, and *foxJ1* mRNAs (Fig. 5*A*). These results were validated by whole-mount in situ hybridization of RNA transcripts (*SI Appendix*, Fig. S12*A*).

We then sought to determine the transcriptional effect of knocking down *rnf20* on *Xenopus* development from fertilization through the LRO stage. We collected RNA hourly in scrambled

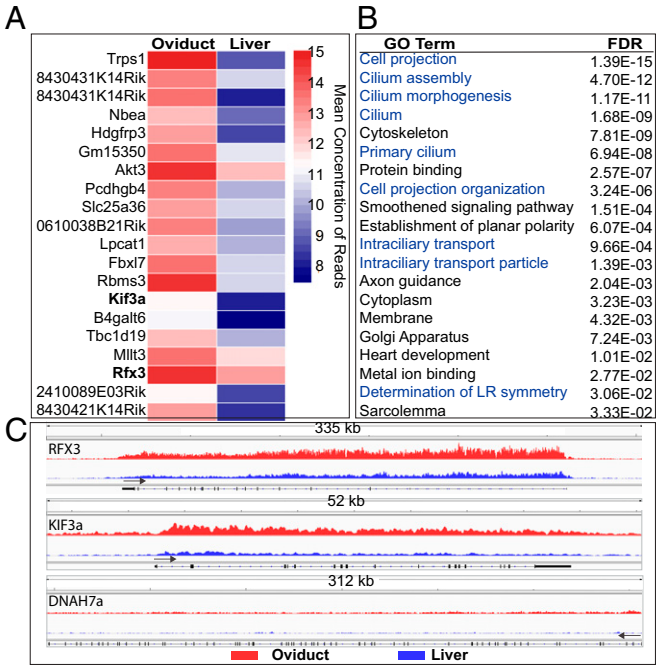

Fig. 4. H2Bub1 marks are enriched at cilia genes in multiciliated tissue. (*A*) A heatmap depicting the top 20 significant regions with increased H2Bub1 occupancy in multiciliated tissue compared with nonciliated tissue. The bolded genes are cilia-related genes depicted in *C*. (*B*) The top 20 significant gene ontology terms from the regions that have increased H2Bub1 occupancy in multiciliated tissue compared with nonciliated tissues. The cilia-related gene ontology terms are shown in blue. (*C*) The H2Bub1 binding profile, depicted using fold enrichment against random distribution values ranging from 0 to 10, across the *Rfx3*, *Kif3a*, and *Dnah7* genes in multiciliated tissue (oviduct; red) and nonciliated tissue (liver; blue). The arrows indicate the TSS and the direction of transcription.

control MO (two replicates) and *rnf20* MO-injected embryos (three replicates) from 1 h post fertilization until 18 h post fertilization (*SI Appendix*, Fig. S11*A*) and performed RNA-seq (*SI Appendix*, Fig. S11*B* and Dataset S2). The data revealed that expression of the mRNAs for ciliary TF *rfx3* and IDA *dnah7*, but not other dynein arm components, was decreased in the *rnf20*-depleted embryos at LRO stages (*SI Appendix*, Fig. S12), consistent with the in situ, qPCR data (Fig. 5*A*) and with the patient who lacked IDAs but not ODAs. The changes did not reach significance, likely because ciliated LRO cells represent only a very small fraction of the whole embryo.

We observed a decrease in both *rfx3* and *dnah7* mRNA levels in *rnf20* morphants, but ChIP-seq revealed that only *Rfx3* was prominently marked with H2Bub1 in mouse multiciliated tissue (Fig. 4*C*). To determine if Rfx3 regulates cilia motility genes when Rnf20 is depleted, we overexpressed *rfx3* mRNA in *rnf20* morphants. This rescued *dnah7* mRNA levels as evaluated by in situ hybridization, while it had no effect on *dnah9* mRNA (*SI Appendix*, Fig. S12*A*). To test if *rfx3* rescues cilia motility in *rnf20* morphants, we depleted *rnf20* and tested MCC function as described earlier. Injection of *rfx3* mRNA into *rnf20* morphants partially rescued cilia motility and epidermal flow (Fig. 5*A* and Movie S8). Abnormal *pitx2c* expression was partially rescued by coinjection of *rfx3* mRNA with *rnf20* MO, indicating rescue of LR patterning defects (Fig. 5*A*). These data place Rnf20 upstream of Rfx3 in development of ciliary motility and LR asymmetry through transcriptional activation of a subset of cilia motility genes, including *dnah7* (Fig. 5*B*).

Discussion

We show that RNF20 complex mutations contribute to human CHD, partly by transcriptional regulation of cilia genes at the LRO required for cardiac LR asymmetry. Knockdown of RNF20 complex members in *Xenopus* results in abnormal heart looping, abnormal cilia motility at the LRO and on MCCs, and decreased H2Bub1 during development at time points corresponding to LRO and MCC formation. H2Bub1 marks are enriched on the *Rfx3* gene in mouse multiciliated tissue. Exogenous *rfx3* mRNA partially rescues the cilia motility and laterality phenotypes resulting from Rnf20 knockdown in *Xenopus*. This indicates that Rnf20-mediated H2Bub1 activates *rfx3* transcription, leading to temporally and spatially controlled regulation of motile ciliogenesis that plays an essential role in heart development.

DNMs in chromatin-remodeling genes, including those affecting H2Bub1, have been linked to 2–3% of CHD (2–5), indicating that cardiac development depends on precise control of chromatin marks. Further, *Rnf20*$^{-/-}$ mice are preimplantation embryonic lethal, pointing to an essential role for H2Bub1 in early development (34). The monoallelic nature of mutations in the RNF20 complex in CHD patients implies that while haploinsufficiency for the RNF20 complex permits very early development to occur, later processes including cardiac development are exquisitely sensitive to smaller changes in H2Bub1.

Cilia are essential in establishing cardiac LR asymmetry, and we present data supporting a tissue-specific regulatory role for H2Bub1 on the core ciliary TF Rfx3. Cilia gene promoters are enriched for X-box motifs recognized by the Rfx family of TFs, of which both Rfx2 and Rfx3 affect LR patterning (22, 23, 35) by transcriptionally regulating cilia genes, including dyneins (20). We found that Rnf20 knockdown affects the expression of *Rfx3* but not *Foxj1* or *Rfx2*, suggesting that *Rfx2* and *Rfx3* are independently

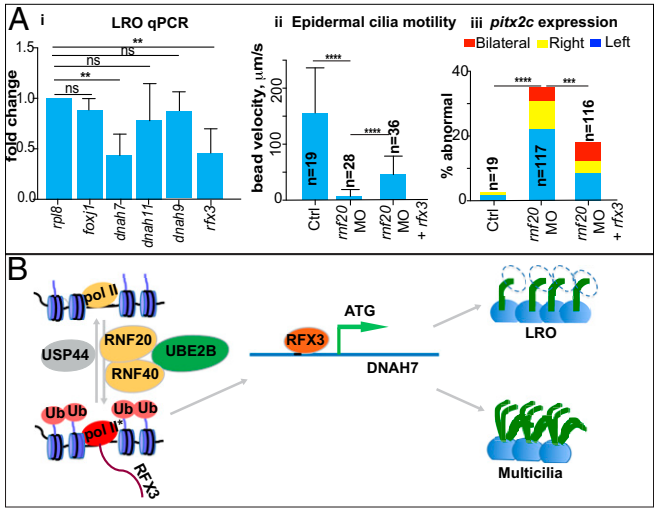

Fig. 5. Transcription factor Rfx3 is downstream of Rnf20. (*A*, *i*) Quantitative RT-PCR of cilia-related genes in the *Xenopus* LRO: *foxj1*, *dnah7*, *dnah9*, *dnah11*, and *rfx3*. Levels of expression are normalized to *rpl8* (ribosomal protein 8). Data are shown as mean ± SEM ($n = 3$). Unpaired *t* test, $^{**}P < 0.00$. (*A*, *ii*) Quantification of epidermal fluid flow across the *Xenopus* multiciliated epithelium in Ctrl, *rnf20* MO, and *rnf20* MO + *Rfx3* mRNA coinjection at the one-cell stage. Mean ± SEM ($n = 3$). *n*, number of embryos. $^{****}P < 0.00005$ (*Left*). (*A*, *iii*) Percentage of embryos with abnormal *pitx2c* after either Ctrl, *rnf20* MO, or *rnf20* MO + *Rfx3* mRNA coinjection at the one-cell stage. Mean ± SEM ($n = 3$). *n*, number of embryos. $^{***}P < 0.0005$, $^{****}P < 0.00005$ (*Right*). (*B*) Proposed mechanism of RNF20 control of cilia motility. E3 ligase RNF20 together with other members of the H2B120K ubiquitination complex selectively ubiquitinates H2B120K at the RFX3 locus, transcriptionally activating RFX3. RFX3, known master regulator of ciliary genes, then drives expression of DNAH7, a motor protein component of the ciliary IDAs required for cilia motility.

regulated and may control some of the tissue-specific expression of cilia components. For example, different ciliated tissues express different subsets of axonemal dyneins that control the specific ciliary beat pattern(s) required in different settings, such as mucociliary clearance in the respiratory tract compared with movement of nonviscous extraembryonic fluid at the LRO (13, 36). It is possible that tissue-specific H2Bub1 levels fine-tune the precise complement of cilia motility proteins.

Our observation of a combinatorial effect on cilia motility and LR patterning resulting from simultaneous knockdown of multiple complex components supports that H2Bub1, rather than any gene-specific effect, is critical for regulating cilia motility gene transcription. H2Bub1 requires a heterodimeric complex consisting of the E3 ligases RNF20 and RNF40 that mediates transfer of ubiquitin from the E2 ligase to the H2B substrate. Vertebrates have two highly homologous E2 ligases, UBE2A and UBE2B. Our data that knockdown of UBE2B alone does not result in a significant developmental phenotype or change in H2Bub1 levels are consistent with data in NIH 3T3 cells (11) and mice (37) that show only mild effects on H2Bub1 with knockdown of UBE2B, in contrast to a severe effect with either knockdown of UBE2A or UBE2A/UBE2B. The redundant, dose-dependent roles of UBE2A and UBE2B point to biological complexity in the mechanism of RNF20 complex-mediated H2Bub1 that is also supported by the observation that humans with haploinsufficiency for RNF20 complex components survive, albeit with significant developmental abnormalities.

Cilia are required at several steps of cardiac development; motile cilia are essential at the LRO to direct asymmetric development of the heart, including atrial asymmetry, direction of heart looping, and directionality of septation of the outflow tract (1, 3, 12). The complete role of RNF20 complex-driven H2Bub1 in cardiac development is likely more complex than by transcriptional regulation of cilia motility at the LRO alone. Notably, the patients with RNF20 complex mutation have a broad spectrum of CHD, and RNF20 complex members are expressed during mouse heart development (*SI Appendix*, Figs. S1*B* and S2 and Table S1) (3). This suggests that the RNF20 complex also functions at other stages of heart development, potentially via biogenesis and function of intracardiac cilia or through extraciliary function in transcriptional regulation of genes required in cardiac development. The findings reported here link the two functional gene ontologies that have been directly implicated in human CHD: chromatin remodeling and cilia function.

Methods

Xenopus and mouse methods and materials (husbandry, MO sequences, and antibodies) are listed in *SI Appendix, Methods*. This includes a detailed description of embryo microinjection, immunohistochemistry, cilia length measurements, video microscopy, in situ hybridization, Western analysis, ChIP-seq and ChIP-qPCR, and computational methods. Mouse and *Xenopus* work was approved by the Yale University Institutional Animal Care and Use Committee. Patient data was obtained as part of the Pediatric Cardiac Genomics Consortium, and all subjects or their parents provided informed consent.

ACKNOWLEDGMENTS. We thank the patients and their families who are the inspiration for this study, Sarah Kubek and Michael Slocum for animal husbandry, and the Center for Cellular and Molecular Imaging at Yale for confocal imaging. This work was supported by a pilot project as part of NIH/National Heart Lung and Blood Institute (NHLBI) 5U01HL098188, NIH/NHLBI 5UM1HL098162, and NIH/NHLBI 5R01HL125885 (to M.B.), NIH/NHLBI U01HL098163 (to W.K.C.), NIH/NHLBI UM1HL098147 and HHMI (to C.E.S.), NIH/NHLBI UM1HL098123 (to B.D.G.), and NIH/*Eunice Kennedy Shriver* National Institute of Child Health and Human Development R01HD081379 and NIH/NHLBI R33HL120783 (to M.K.K.). M.K.K. is a Mallinckrodt Scholar. The contents of this publication are solely the responsibility of the authors and do not necessarily represent the official views of the NHLBI.

1. M. E. Pierpont *et al.*; American Heart Association Council on Cardiovascular Disease in the Young; Council on Cardiovascular and Stroke Nursing; Council on Genomic and Precision Medicine, Genetic basis for congenital heart disease: Revisited: A scientific statement from the American Heart Association. *Circulation* **138**, e653–e711 (2018).
2. J. Homsy *et al.*, De novo mutations in congenital heart disease with neurodevelopmental and other congenital anomalies. *Science* **350**, 1262–1266 (2015).
3. S. C. Jin *et al.*, Contribution of rare inherited and de novo variants in 2,871 congenital heart disease probands. *Nat. Genet.* **49**, 1593–1601 (2017).
4. A. Sifrim *et al.*; INTERVAL Study; UK10K Consortium; Deciphering Developmental Disorders Study, Distinct genetic architectures for syndromic and nonsyndromic congenital heart defects identified by exome sequencing. *Nat. Genet.* **48**, 1060–1065 (2016).
5. S. Zaidi *et al.*, De novo mutations in histone-modifying genes in congenital heart disease. *Nature* **498**, 220–223 (2013).
6. S. Y. Ang *et al.*, KMT2D regulates specific programs in heart development via histone H3 lysine 4 di-methylation. *Development* **143**, 810–821 (2016).
7. J. A. Wamstad *et al.*, Dynamic and coordinated epigenetic regulation of developmental transitions in the cardiac lineage. *Cell* **151**, 206–220 (2012).
8. S. Chen, J. Li, D. L. Wang, F. L. Sun, Histone H2B lysine 120 monoubiquitination is required for embryonic stem cell differentiation. *Cell Res.* **22**, 1402–1405 (2012).
9. G. Fuchs *et al.*, RNF20 and USP44 regulate stem cell differentiation by modulating H2B monoubiquitylation. *Mol. Cell* **46**, 662–673 (2012).
10. O. Karpiuk *et al.*, The histone H2B monoubiquitination regulatory pathway is required for differentiation of multipotent stem cells. *Mol. Cell* **46**, 705–713 (2012).
11. J. Kim *et al.*, RAD6-mediated transcription-coupled H2B ubiquitylation directly stimulates H3K4 methylation in human cells. *Cell* **137**, 459–471 (2009).
12. Y. Li *et al.*, Global genetic analysis in mice unveils central role for cilia in congenital heart disease. *Nature* **521**, 520–524 (2015).
13. J. McGrath, S. Somlo, S. Makova, X. Tian, M. Brueckner, Two populations of node monocilia initiate left-right asymmetry in the mouse. *Cell* **114**, 61–73 (2003).
14. S. Nonaka *et al.*, Randomization of left-right asymmetry due to loss of nodal cilia generating leftward flow of extraembryonic fluid in mice lacking KIF3B motor protein. *Cell* **95**, 829–837 (1998).
15. A. Schweickert *et al.*, Cilia-driven leftward flow determines laterality in *Xenopus*. *Curr. Biol.* **17**, 60–66 (2007).
16. S. Yuan, L. Zhao, M. Brueckner, Z. Sun, Intraciliary calcium oscillations initiate vertebrate left-right asymmetry. *Curr. Biol.* **25**, 556–567 (2015).
17. B. A. Afzelius, A human syndrome caused by immotile cilia. *Science* **193**, 317–319 (1976).
18. M. P. Kennedy *et al.*, Congenital heart disease and other heterotaxic defects in a large cohort of patients with primary ciliary dyskinesia. *Circulation* **115**, 2814–2821 (2007).
19. S. L. Brody, X. H. Yan, M. K. Wuerffel, S. K. Song, S. D. Shapiro, Ciliogenesis and left-right axis defects in forkhead factor HFH-4-null mice. *Am. J. Respir. Cell Mol. Biol.* **23**, 45–51 (2000).
20. L. El Zein *et al.*, RFX3 governs growth and beating efficiency of motile cilia in mouse and controls the expression of genes involved in human ciliopathies. *J. Cell Sci.* **122**, 3180–3189 (2009).
21. J. L. Stubbs, I. Oishi, J. C. Izpisúa Belmonte, C. Kintner, The forkhead protein Foxj1 specifies node-like cilia in *Xenopus* and zebrafish embryos. *Nat. Genet.* **40**, 1454–1460 (2008).
22. B. W. Bisgrove, S. Makova, H. J. Yost, M. Brueckner, RFX2 is essential in the ciliated organ of asymmetry and an RFX2 transgene identifies a population of ciliated cells sufficient for fluid flow. *Dev. Biol.* **363**, 166–178 (2012).
23. M. I. Chung *et al.*, RFX2 is broadly required for ciliogenesis during vertebrate development. *Dev. Biol.* **363**, 155–165 (2012).
24. I. K. Quigley, C. Kintner, Rfx2 stabilizes Foxj1 binding at chromatin loops to enable multiciliated cell gene expression. *PLoS Genet.* **13**, e1006538 (2017).
25. M. Foglizzo, A. J. Middleton, C. L. Day, Structure and function of the RING domains of RNF20 and RNF40, dimeric E3 ligases that monoubiquitylate histone H2B. *J. Mol. Biol.* **428**, 4073–4086 (2016).
26. K. E. Samocha *et al.*, A framework for the interpretation of de novo mutation in human disease. *Nat. Genet.* **46**, 944–950 (2014).
27. D. Szklarczyk *et al.*, The STRING database in 2017: Quality-controlled protein-protein association networks, made broadly accessible. *Nucleic Acids Res.* **45**, D362–D368 (2017).
28. K. Kosaki *et al.*, Absent inner dynein arms in a fetus with familial hydrocephalus-situs abnormality. *Am. J. Med. Genet. A* **129A**, 308–311 (2004).
29. P. Vick *et al.*, Flow on the right side of the gastrocoel roof plate is dispensable for symmetry breakage in the frog *Xenopus laevis*. *Dev. Biol.* **331**, 281–291 (2009).
30. A. K. Ryan *et al.*, Pitx2 determines left-right asymmetry of internal organs in vertebrates. *Nature* **394**, 545–551 (1998).
31. A. Schweickert *et al.*, The nodal inhibitor Coco is a critical target of leftward flow in *Xenopus*. *Curr. Biol.* **20**, 738–743 (2010).
32. D. Bhattacharya, C. A. Marfo, D. Li, M. Lane, M. K. Khokha, CRISPR/Cas9: An inexpensive, efficient loss of function tool to screen human disease genes in *Xenopus*. *Dev. Biol.* **408**, 196–204 (2015).
33. Y. J. Zhang *et al.*, Identification of dynein heavy chain 7 as an inner arm component of human cilia that is synthesized but not assembled in a case of primary ciliary dyskinesia. *J. Biol. Chem.* **277**, 17906–17915 (2002).
34. O. Tarcic *et al.*, RNF20 links histone H2B ubiquitylation with inflammation and inflammation-associated cancer. *Cell Rep.* **14**, 1462–1476 (2016).
35. E. Bonnafe *et al.*, The transcription factor RFX3 directs nodal cilium development and left-right asymmetry specification. *Mol. Cell. Biol.* **24**, 4417–4427 (2004).
36. G. W. Dougherty *et al.*, DNAH11 localization in the proximal region of respiratory cilia defines distinct outer dynein arm complexes. *Am. J. Respir. Cell Mol. Biol.* **55**, 213–224 (2016).
37. H. P. Roest *et al.*, The ubiquitin-conjugating DNA repair enzyme HR6A is a maternal factor essential for early embryonic development in mice. *Mol. Cell. Biol.* **24**, 5485–5495 (2004).